applied sciences

MDPI

Article

Study of Static and Dynamic Properties of Sand under Low Stress Compression

Vladimir Frid [1,*], Stelios M. Potirakis [2,*] and Semen Shulov [1]

[1] Civil Engineering Department, Sami Shamoon College of Engineering, Jabotinsky 84, Ashdod 77245, Israel; semiosh1@ac.sce.ac.il
[2] Department of Electrical and Electronics Engineering, University of West Attica, 12244 Egaleo-Athens, Greece
* Correspondence: vladimirf@ac.sce.ac.il (V.F.); spoti@uniwa.gr (S.M.P.)

Abstract: The aim of this work was to investigate a wide range of grain sizes of sand in the pre-yield regime during compression through the combined study of ultrasound (US) wave speed and acoustic emission (AE). The specific study was performed using modified oedometer and uniaxial compression experimental set-ups. The studied samples were natural dune sand (poorly graded on the poorly graded sand (SP) index) as well as its three extracted fractions as follows: 2.36–0.6 mm, 0.6–0.3 mm and 0.3–0.075 mm. The maximum compression stress during the modified oedometer experiments was <150 kPa, while during the modified uniaxial compression experiments, it was <400 kPa. Each sample was loaded while measuring the US pressure (P) wave speed and AE at each loading stage. The results show that the stiffer the soil is, the higher the value of the P wave speed measured, resulting in similar P wave velocity values achieved at a much lower applied stress during the oedometer experiments in comparison with the uniaxial compression tests. Regarding the AE results, it is seen that the higher the stress level is, causing more friction between the sand particles, the more AE events there are during their movement. The following parameters of AE were shown to be the most sensitive to the stress increase: the number of AE hits and the signals' energy.

Keywords: acoustic emission; ultrasound wave speed; sand; compression experiments

Citation: Frid, V.; Potirakis, S.M.; Shulov, S. Study of Static and Dynamic Properties of Sand under Low Stress Compression. *Appl. Sci.* **2021**, *11*, 3311. https://doi.org/10.3390/app11083311

Academic Editor: Edoardo Piana

Received: 8 March 2021
Accepted: 31 March 2021
Published: 7 April 2021

1. Introduction

Numerous studies of the acoustic emission (AE) phenomenon make it possible to understand that the AE signals are small-scale events whose properties are similar to the large-scale radiation of an elastic wave caused by earthquakes [1–9]. It has been shown that the AE time sequence parameters correspond well with the evolution of the rupture events [2,3,10,11]. Presently, AE is the standard method for the assessment of the material stress condition [12–14]. Michlmayr et al. [15] reviewed six mechanisms of AE, part of which were more or less common for different materials, while others were inherent to some specific materials and conditions. For example, AE produced in soils (when they are dry) can be associated with crack development, grain friction, grain cementation fracture (for cemented soils) and liquid bridge rupture (when the soil is wet or saturated).

AE studies during soil loading in laboratory conditions are less common than studies during rock destruction ([16] and references therein). It is known that sand samples under load behave in three regimes [17]—the pre-yield, the clastic and the stiffness regain—while the mechanism of deformation depends on the load level. For example, during the pre-yield regime, the sand stiffness increases due to rolling and sliding between particles, following a more rigid arrangement of particles. Fernandes et al. [18] studied three types of coarse sand samples with a low height to sample diameter ratio (HtD = 0.3). The AE was characterized by counting the number of times when the signal amplitude exceeded a given threshold. Experiments have shown that the obtained AE signals can be used to detect the onset of the clastic and stiffness regain regimes [17]. Lin et al. [19] noted that the generation of lower frequency AE components (below 100 kHz), medium-high frequency

AE components (100–200 kHz) and high-frequency components (200–700 kHz) during sand compression resulted from different modes of micromechanical behaviors of particle readjustment, asperity abrasion and microcracking, respectively. Lin et al. [20] studied sandy soils subjected to triaxial compression. The AE hit number and AE hit rate were used as the AE parameters. A similarity was observed between the relation's stress vs. strain and the AE hit rate vs. strain. It was shown that an increased confining stress or initial relative density caused more AE signals. The authors noted the effect of the failure mechanism under the same values of confining stress: more AE signals were recorded in loose sands that failed due to swelling than in densely compacted sands which failed due to shear banding. Note the discrepancy between the results by Lin et al. [20] and those by Mao et al. [16]. It has also been found that the peak of the AE hit rate was not always synchronous with the peak of the stress but fluctuated around it. Naderi-Boldaji et al. [21] studied the AE behavior during soil compression using an oedometer. The sandy samples (HtD $\approx$ 1) including 12% and 25% water content were studied. A close correspondence was found between the number of AE hits, their energy and the soil strain–stress conditions.

It was noted in [22] that AE parameters vary significantly depending on the material properties, the strength of the signal and background noise, among other factors. Thus, it is difficult to select the most valuable parameter (or combination of parameters) for the characterization of a failure process.

Alternative non-destructive techniques which are generally utilized for microfracturing characterization in granular media are 3D microscopy and X-ray or neutron tomography imaging [23]. These methods allow for reaching results with high spatial resolutions, but their application is very limited at the geophysical scale due to intrinsic restrictions in the examination depth, their use only in the postpone mode, their high time consumption and their significant cost. The advantage of the AE method is its ability to characterize the destruction of different materials at all spatial scales and during the failure process itself [1–15].

Moreover, the AE method, as well as any geophysical method being an indirect tool for failure characterization, has its own restrictions. The way to overcome such limitations is to combine the AE results with the results of another method based on a different physical phenomenon for a comprehensive study.

Ultrasound (US) is the standard method for assessing dynamic properties in various materials [24]. For example, Stephenson [25] studied the dynamic Young and shear moduli of soil using the US method. Zimmer et al. [26] measured the P and shear (S) wave speeds in the samples of dry and water-saturated natural sand samples. The exponent relationships between the P wave speed and the applied external load were found. Chen et al. [27] studied the elastic wave velocity of an unsaturated silty sand.

The difference in the AE and US behavior in four types of sand was studied in [28]. It was shown that when the stress level gradually increased, the US wave speed gradually increased as well, while the AE activity was sharply excited. On the other hand, during stress relaxation, the US wave speed abruptly decreased while the AE activity was minor. Such a dissimilarity in the behavior of US and AE phenomena renders them obvious candidates for the comprehensive study of sand under compression.

The state-of-the-art analysis portrays that most studies of granular material loading have been carried out (1) with only one loading tool (e.g., oedometer) [18,21,29] or different types of compression machines or shear machines [20,29–33], (2) typically under high compression stress (i.e., in the clastic and stiffness regain regimes) (e.g., [29,32]) or during individual grains fracturing [19,23,34] and (3) for a very thin range of grain sizes (e.g., [22] and references therein). In addition, there are no widely agreed valuable parameters of AE to characterize sand stress–strain behavior under low stress. The studies of granular materials under low stress are significantly rare (e.g., [28,30], as well as the combined study of US and AE measurements [28,33]). All the above reflect the knowledge gap in the field. The goal of this paper is to fill the existing knowledge gap.

This paper presents the novel results of the following:

1. The comparison of sand loading using an oedometer and an uniaxial compression machine in the pre-yield regime (under low stress), in terms of combined AE and US measurements;
2. The analysis of sensitivity of different time domain AE parameters to the stress–strain changes;
3. The loading of the wide range of sand grain sizes of 0.075–4.75 mm (natural poorly graded dune sand) as well as its three extracted fractions as follows: 2.36–0.6 mm, 0.6–0.3 mm and 0.3–0.075 mm.

Emphasis is put on the differences in stress–strain behavior of the four types of sand under loading, using these two types of loading tools with a special focus on the US and AE characteristics.

The outcome of this study can be utilized in geomechanics to understand the stability of shallow infrastructure systems such as pipelines, foundations and retaining structures. For example, Mao et al. [16] in their Figure 1 presented a "typical failure pattern and the relevant load-displacement curves for shallow foundations resting on soil", while the most sensitive parameters observed in this paper may be used for the short-term assessment of load degree in the future. In addition, the results of this paper can be the basis for a future study of different aspects of the liquefaction process, soil sliding (e.g., [30,31] and references therein) and sinkhole creation. For example, sinkholes in the region of the Dead Sea present a permanent hazard for the industrial and touristic facilities. Figure 1 shows a heavy factory construction in the Dead Sea region, where the problem of short-term estimation of constructions' stability due to sinkhole creation just beneath them still remains unsolved.

Figure 1. An example of a heavy industrial facility in the sinkhole hazardous zone.

2. Materials and Methods

2.1. Methods

The outline of this research, according to the reasoning already presented in the introduction (Section 1), is shown in Figure 2 in the form of a block diagram. This study consists of three types of experiments, and they are as follows: (1) a modified oedometer test using dry sand samples (OD hereafter), HtD < 1; (2) a modified uniaxial compression test with passive confinement using dry sand samples (UCD); and (3) a modified uniaxial compression test with passive confinement using wet sand samples (UCW). The HtD for UCD and UCW was ≈2 (see the following for more explanation). Figure 3a,b shows the experimental setups for these three types of tests.

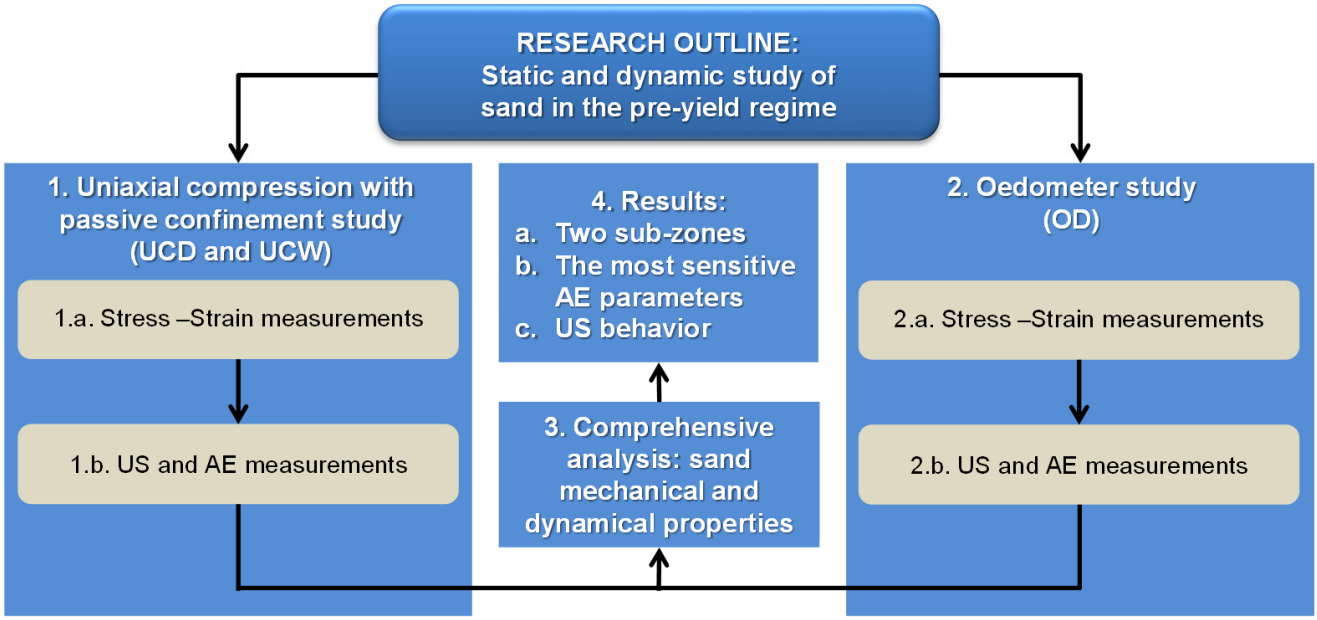

Figure 2. Block diagram presenting the research outline. The key objective of this research was the comprehensive experimental study of the mechanical and dynamical properties of sand in the pre-yield regime by means of combined acoustic emission (AE) and ultrasound (US) analysis.

The oedometer loading system (Matest S.p.A, Treviolo BG, Italy) was used as the basis for the OD experiments (Figure 3a). The used load cell (blue cylindrical ring in Figure 3a) allowed vertical deformation of the soil sample, restricting its horizontal extension. The inner diameter of the load cell was 51.6 mm, while its height was 31.5 mm. The sample was incrementally loaded via its top end while its bottom end was in a fixed condition. The load increment was 5 kg. The maximum load applied to the samples was 30 kg, corresponding to an applied stress level of 143.5 kPa. At each increment of loading, the final deformation value was measured using a displacement gauge (Figure 3a).

The loading system (ELE International, Leighton Buzzard, UK), modified for uniaxial compression by using a steel load cell, was used as the basis for the UCD and UCW experiments (Figure 3b). The load cell (black cylindrical ring in Figure 3b) allowed vertical deformation of the soil sample, restricting its horizontal extension. The internal diameter of the load cell was 38.6 mm, while its height was 71.1 mm. The sample was incrementally loaded via its top end while its bottom end was in a fixed position. The load increment was 10 kg (~100 N). The maximum applied stress level was ~350 kPa. At each increment of loading, the final deformation value was measured using a displacement gauge (Figure 3b).

During all three experiments, two US sensors for P wave speed measurement were located at both ends of the soil samples, while the AE sensor was located at the fixed bottom end of the load cell. The generating and receiving US sensors were connected to the pulse generator (TG5011A) and the digital oscilloscope (GDS1054B), respectively (Figure 3a,b).

The resonance frequency of the US sensors was 75 kHz. The Open Wave software was used for data recording to a personal computer (PC). The US wave speed was measured using the first arrivals method.

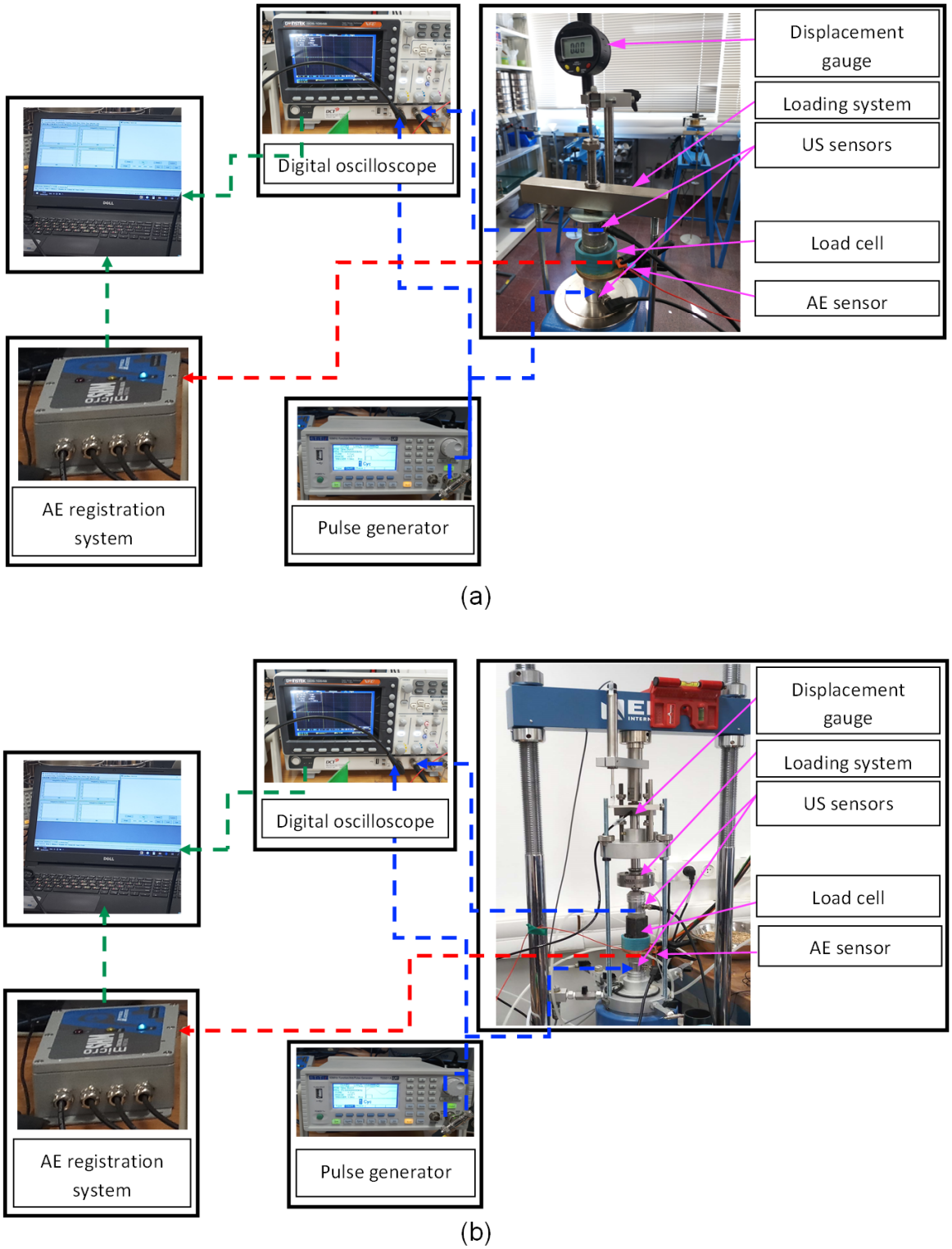

Figure 3. The experimental setup for the ultrasonic and acoustic emission study. (**a**) The oedometer with dry sand samples (OD) test. (**b**) The modified uniaxial compression test with passive confinement using dry sand samples (UCD) and modified uniaxial compression test with passive confinement using wet sand samples (UCW) tests. For the explanation of these abbreviations, see Section 2.1.

The AE sensor was connected to the micro-SHM (Structural Health Monitoring) monitoring system (Mistras/Physical Acoustic Inc, Princeton Jct, NJ, USA). The AEwin for micro-SHM software was used for data recording to the PC. The measurements of AE were restricted by digital filtering in the range of 300–500 kHz to diminish acoustic noise. AE measurements were carried out continuously at each stage of loading while the pulse generator was turned off.

Figure 4a presents an indicative snapshot during one of the modified uniaxial tests with passive confinement, while Figure 4b illustrates an indicative screenshot of the US signals measured by the digital oscilloscope during the specific test and Figure 4c presents an indicative recording of the AE signal.

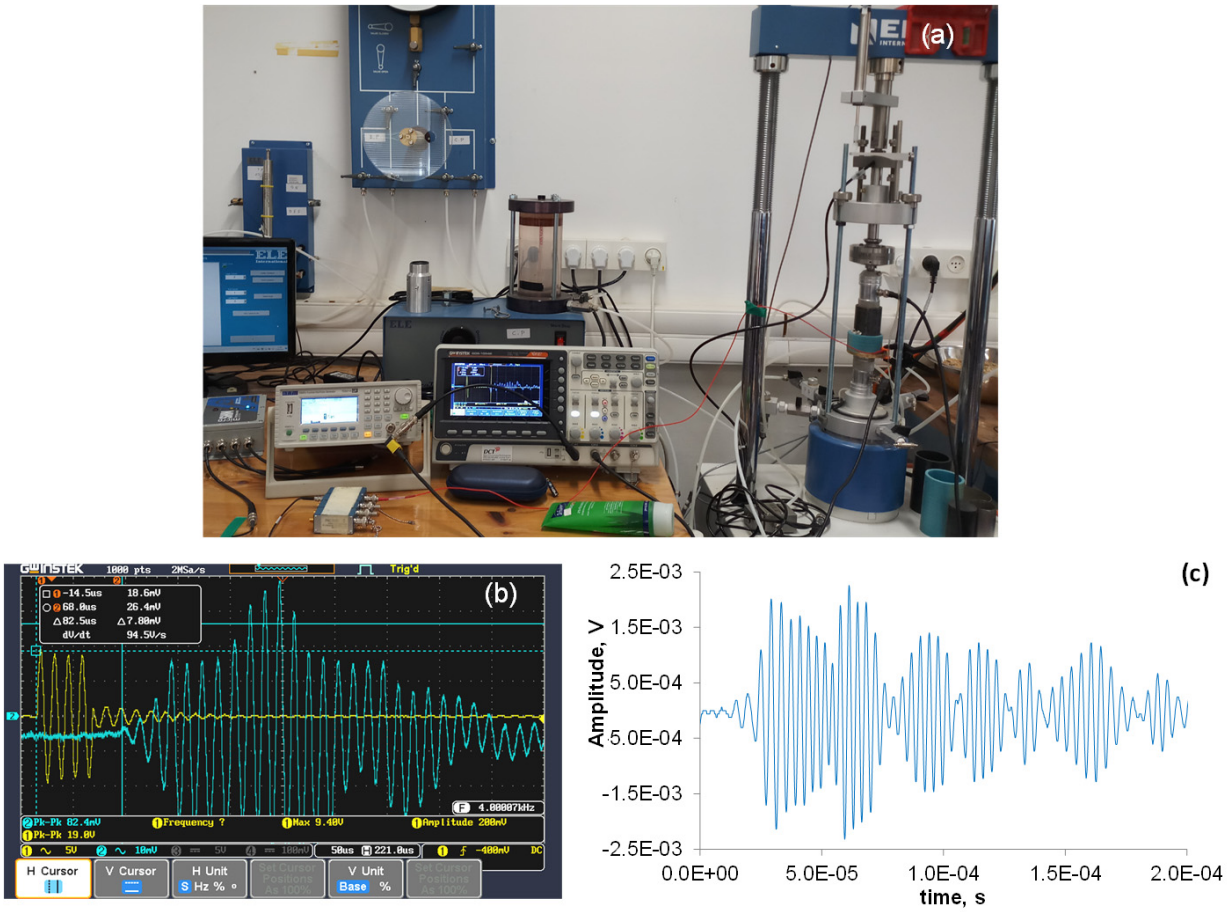

Figure 4. (**a**) Indicative snapshot during one of the modified uniaxial tests with passive confinement. (**b**) Indicative screenshot of the US signals measured by the digital oscilloscope. (**c**) Indicative AE signal acquired during the experiments. Note that in the used number format, the notation "E±xx" is part of a scientific notation and corresponds to "$\cdot 10^{\pm xx}$".

2.2. The Procedure of Sample Preparation

Dune sand from the Ashdod beach (southern Israel) was selected for the experiments. Grain distribution analysis showed that the sand could be categorized as sand, poorly graded (SP), based on the Unified Soil Classification System (USCS). The experiments were carried out using four types of samples as follows: natural dune sand and its three extracted fractions (2.36–0.6, 0.6–0.3 and 0.3–0.075 mm (Figure 5a,b)). Note that the selected grain size was significantly wider than in the majority of other investigations that mainly used a very thin range of grain sizes ([22] and references therein). Prior to sample preparation, all types of sand were dried for 24 h in an oven at 105 °C (Figure 5c). After the sand samples were dried, they were placed in the OD and UCD or UCW loading cells (Figure 5d,e, respectively). The average beginning value of the density for all dry samples was 1.67 ± 0.03 gr/cm^3,

while for wet samples it was 1.79 ± 0.03 gr/cm^3. The value of the mass moisture content in the UCW tests was experimentally selected to be 5%, which was the maximum moisture content that could be absorbed by the sandy material but not squeezed out during sample preparation. The values of the mass moisture content were checked by the standard method of moisture content observation [35]. In addition, the open porosity n of the soil samples can be calculated as follows:

$$n = 1 - \frac{sample\ density}{quartz\ density} \quad (1)$$

Figure 5. (**a**) The lab tools used for sand sieving and weighting. (**b**) The photos of the sand fractions used for the study. (**c**) The sand samples in the oven prior to drying. (**d**) The load cell for the OD study, including the filter and pore stone. (**e**) The load cell for the UCD and UCW studies, including the filter and pore stone.

The value of the quartz density was known to be 2.65 gr/cm^3; hence, the estimated values of open porosity for the dry and wet samples were $n_{dry} = 0.37$ and $n_{wet} = 0.32$, with the difference between them being 0.05. This value was equal to the value of the mass moisture content noted above.

3. Results

3.1. Two Sub-Zones of Sample Deformation

Figures 6–14 show the stress–strain curves for the three types of experiments (OD, UCD and UCW; see Section 2.1) and four kinds of sand samples (natural dune sand and its three extracted fractions: 2.36–0.6, 0.6–0.3 and 0.3–0.075 mm; see Section 2.2), along with the obtained US and AE measurements. For a more accurate comparison of the results, we distinguished the pre-yield regime into two subzones: subzone 'a', characterized by intensive sand compression (i.e., high changes in strain values with a relatively low increase in stress (at the beginning of the deformation process, the low slope of the strain–stress graph), and subzone 'b', characterized by low changes in the strain with a relatively intense increase in stress (high slope of the strain–stress graph).

It is seen that the size of subzone 'a' was insignificant for the OD experiments (lacking or quite small range of subzone a), significant and very wide for the UCW experiments and visible but of a minor width for the UCD tests (much lower width relative to that of the UCW experiments). The slope of the stress–strain curves in subzone 'b' was very similar for both UCD and UCW experiments, while it was much lower for the OD experiments.

3.2. The Results of US Measurements

Figure 6 shows the results of the US measurements. The analysis of Figure 6 yielded the following information. Concerning the P wave range, (1) the P wave speed increased with the rise in the stress level, while (2) the range of the P wave speed was similar for all studied sand samples and all three types of tests, being 400–850 m/s, while the value of the speed was mainly determined by stress growth (see Figure 6b) and not by the strain rise. Comparing the OD and UCD results, one can observe that the value of the applied vertical stress, which was necessary to reach similar values of the P wave speed, was lower for the OD test than for the UCD tests, but the value of the realized strain was similar. Note the similar diapason of the P wave speed values for both tests. By comparing the UCD results against the UCW results, it is seen that during both experiments, the range of the P wave speed was similar for all types of sand, while the value of induced strain was much higher during the UCW experiments relative to those during the UCD experiments (mainly due to the size of subzone a).

3.3. The Results of AE Measurements

In the following, we present the AE measurement results for each AE parameter. Specifically, the AE hit number, as well as eight parameters of individual AE hits, were studied. The most comprehensive description of these parameters is presented in [12,13,21,34]. Here, only their brief definitions are provided as follows: The rise time is the time from the first threshold crossing to the highest voltage on the waveform (μs); counts refers to the number of times that the signal crosses the detection threshold during its entire duration; energy is the time integral of the absolute signal voltage; the duration of the AE hit is the time from the first to the last threshold crossing (μs); the amplitude is the highest voltage in the AE waveform, expressed on the AE_{dB} amplitude scale; the average frequency is the counts divided by the duration (divided by 1000, thus the expression in kHz), and this parameter is calculated from the time domain features (not spectral); the peak number is the number of cycles that exceeds the threshold in the rise time period of the AE hit; and the abs-energy is the time integral of the signal voltage at the sensor before any amplification, divided by a 10 kΩ impedance and expressed in aJ (attoJoules; 10^{-18} Joules).

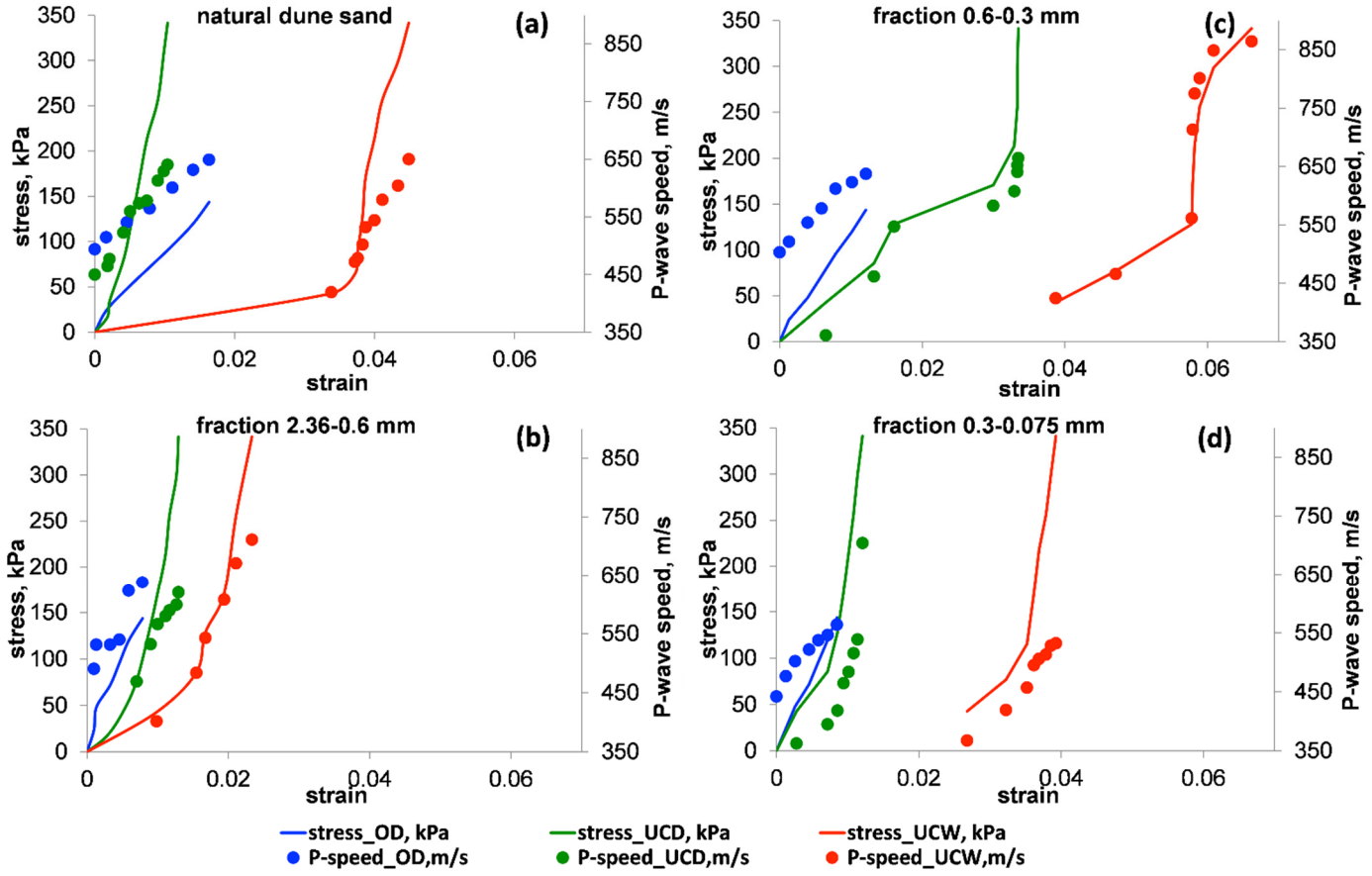

Figure 6. The stress–strain relationships (solid curves) vs. the values of the US P wave speed (full circles) for the OD (blue), UCD (green) and UCW (red) tests. Panels (**a**–**d**) show the results for natural dune sand and its three extracted fractions as follows: 2.36–0.6, 0.6–0.3 and 0.3–0.075 mm, respectively.

The above-mentioned eight parameters (except the AE hits number) were studied in two ways:

1. The cumulative number of each parameter at a loading stage ($\sum Y_i$, where Y means the parameter studied, while the index i means that summation was done for $i-$ loading stage;
2. The average value $\overline{Y}$ of a parameter per AE hits number at $i-$ loading stage, such that $\overline{Y} = \sum Y_i / \sum NH_i$, where NH means the number of hits at a loading stage, while index i means that summation was done for the value $i-$ loading stages.

3.3.1. AE Hit Number

Figure 7 shows the results of AE registration (the number of AE hits per loading stage and the cumulative number of AE hits). From Figure 7, it is seen that the higher stress level was, the greater the number of AE hits registered (see the cumulative graphs of the AE hit numbers for all experiments, the full circles in Figure 7). The number of AE hits appearing at each loading stage tended to increase with an increasing stress level, occasionally deviating from the general trend (see the empty squares in Figure 7). Note that the deviation was not specific to either the test type or the type of sand sample.

One can also observe that most of the AE signals emerged in subzone b for all test types. The analysis of the number of AE hits emanating in subzone a showed that their quantity was generally much higher in the wet sand samples than in the dry sand samples under the corresponding stress level. Moreover, for subzone b, the number of AE hits increased with the stress growth, but it was quite similar in the UCD and UCW tests. The

number of AE hits registered during the OD experiments was lower than in the UCD and UCW experiments, which is consistent with the observation noted above [20,21].

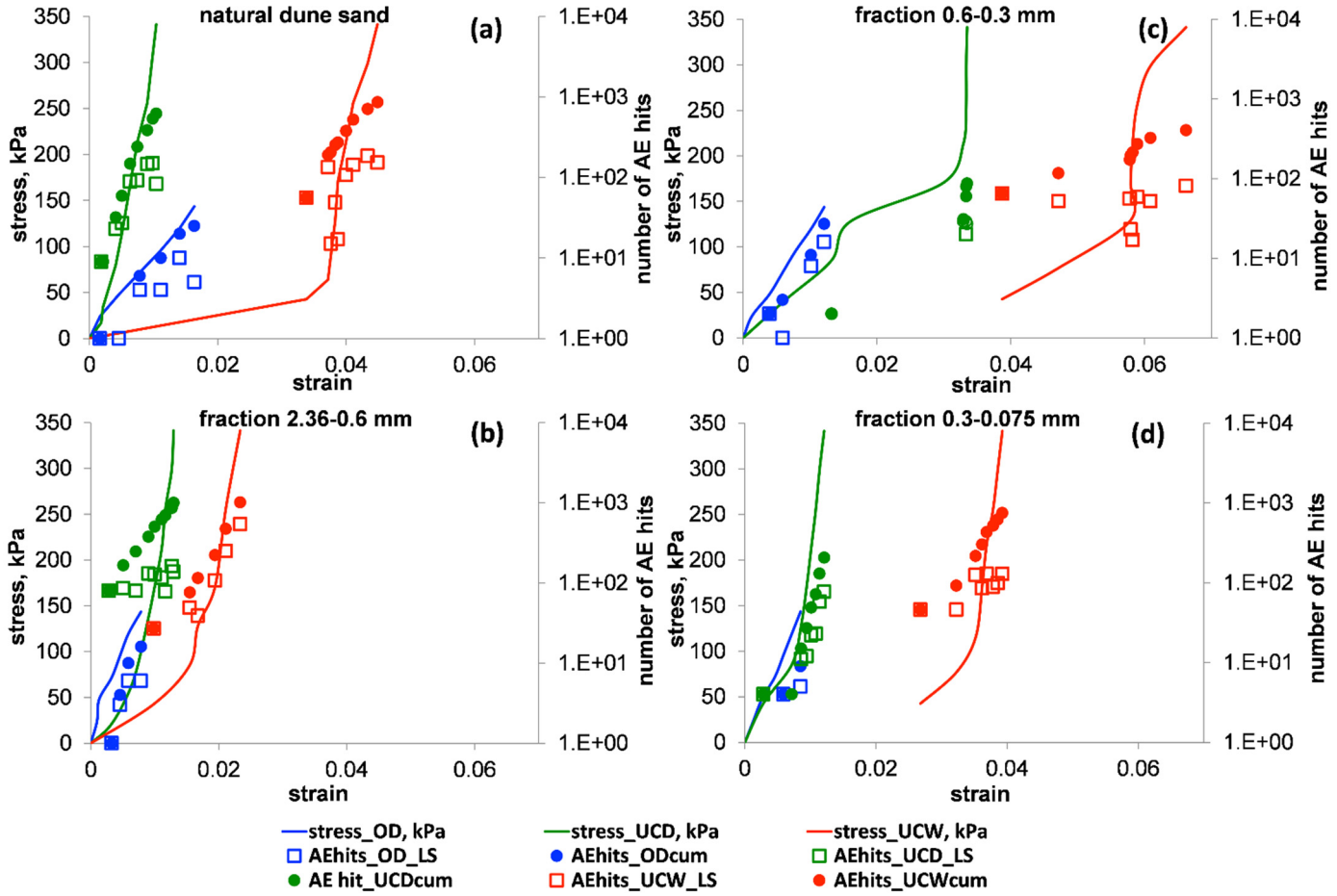

Figure 7. The stress–strain relationships (solid curves) vs. the values of the AE hit number (AEhits) for the OD (blue), UCD (green) and UCW (red) tests. The empty squares and the full circles denote the number of AE hits per loading stage (index = LS) and the cumulative number of AE hits (index = cum), respectively. Panels (**a**–**d**) illustrate the results for natural dune sand and its three extracted fractions: 2.36–0.6, 0.6–0.3 and 0.3–0.075 mm, respectively. Note that in the used number format, the notation "E±xx" is part of a scientific notation and corresponds to "$\cdot 10^{\pm xx}$".

3.3.2. Rise Time

The AE results in terms of the rise time (RT) parameter are shown in Figure 8, from which one can conclude that the value of the average RT was not intensively varied during sample loading (mainly restricted in the range of 10–100 ms). The parameter seemed to be quite independent from the stress level, the type of the test, the sand granularity and the moisture content. Moreover, the cumulative value of the RT for a loading stage increased with the rise in the stress value. The maximum value of the cumulative RT was observed for the UCD test using the coarsest sand fraction.

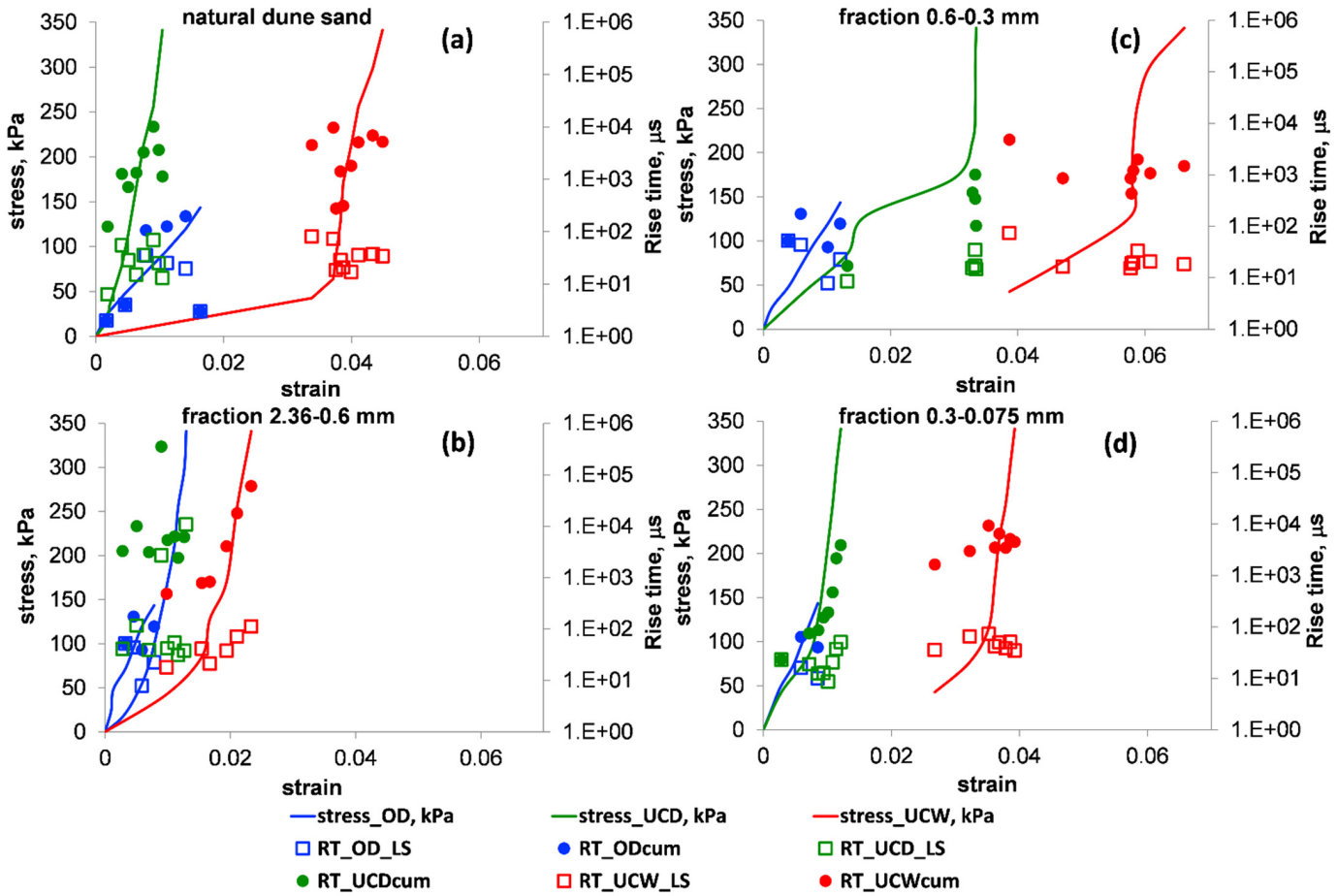

Figure 8. The stress–strain relationships (solid curves) vs. the values of the rise time (RT) for the OD (blue), UCD (green) and UCW (red) tests. The empty squares and the full circles denote the values of average (index = LS) and cumulative (index = cum) RTs for a loading stage, respectively. Panels (**a**–**d**) present the results for natural dune sand and its three extracted fractions: 2.36–0.6, 0.6–0.3 and 0.3–0.075 mm, respectively. Note that in the used number format, the notation "E±xx" is part of a scientific notation and corresponds to "$\cdot 10^{\pm xx}$".

3.3.3. Counts

The AE results in terms of the counts parameter are shown in Figure 9. In Figure 9, it is seen that the value of the average counts per loading stage ranged between 0.1 and 100, where the minor values were measured during the OD experiments while the maximal values were observed during the UCD tests using the coarsest fraction. It can be noted that there was a weak increasing tendency in the value of the average counts per loading stage with the increase in the stress magnitude (e.g., the UCW test with natural dune sand and the finest fraction, as well as the UCD test using the finest fraction). Furthermore, the cumulative value of the counts for each loading stage increased with the increase in the stress level. The maximum number of the cumulative value of the counts for each loading stage was observed for the UCD tests with the coarsest sand fraction. Note that the maximum value of the cumulative count per loading stage was not thoroughly synchronized with the maximum of the applied stress.

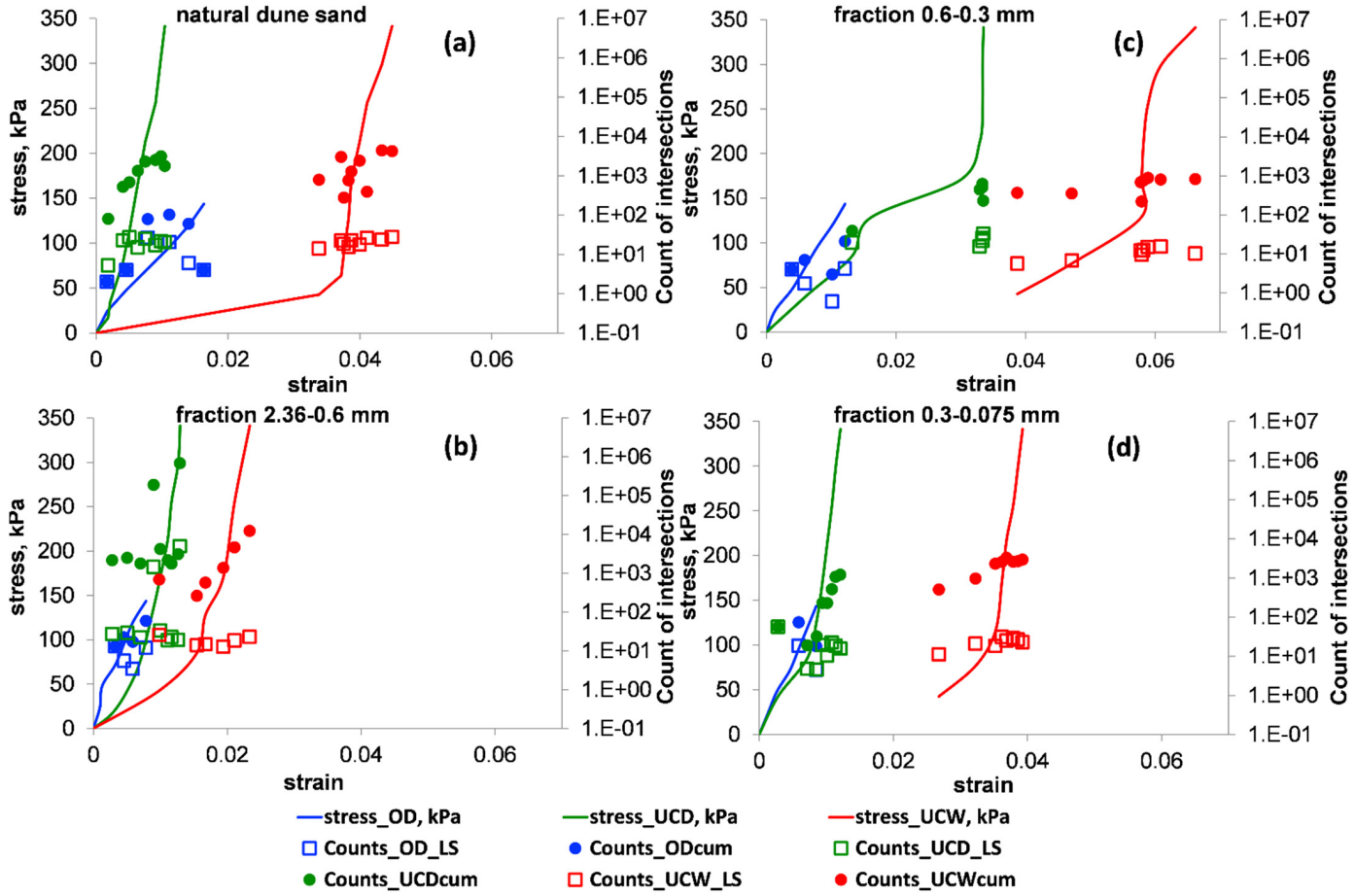

Figure 9. The stress–strain relationships (solid curves) vs. the values of the counts for the OD (blue), UCD (green) and UCW (red) tests. The empty squares and the full circles denote the values of average (index = LS) and cumulative (index = cum) counts for a load stage, respectively. Panels (**a**–**d**) show the results for natural dune sand and its three extracted fractions: 2.36–0.6, 0.6–0.3 and 0.3–0.075 mm, respectively. Note that in the used number format, the notation "E±xx" is part of a scientific notation and corresponds to "$\cdot 10^{\pm xx}$".

3.3.4. Energy

The AE results in terms of the energy parameter are shown in Figure 10. The following information can be drawn from these results. The value of the average energy values per loading had a tendency to increase with an increase in the stress level. The most explicit tendency (for subzone b) was observed for the coarsest fraction in the UCD test (Figure 10b), while the results of the UCW and OD tests showed the same trend as well.

The highest cumulative energy value for each loading step was measured for the coarsest fraction during the UCD experiments (Figure 10b). Comparison the results of the UCD and UCW experiments revealed that the dispersion in cumulative energy values for each loading stage was lower for the UCW tests than for the UCD experiments, while the general tendency toward increasing the absolute value of the energy with the stress growth persisted for all types of sand samples. Note that the maximum value of energy per loading stage did not exactly correspond to the maximum stress value.

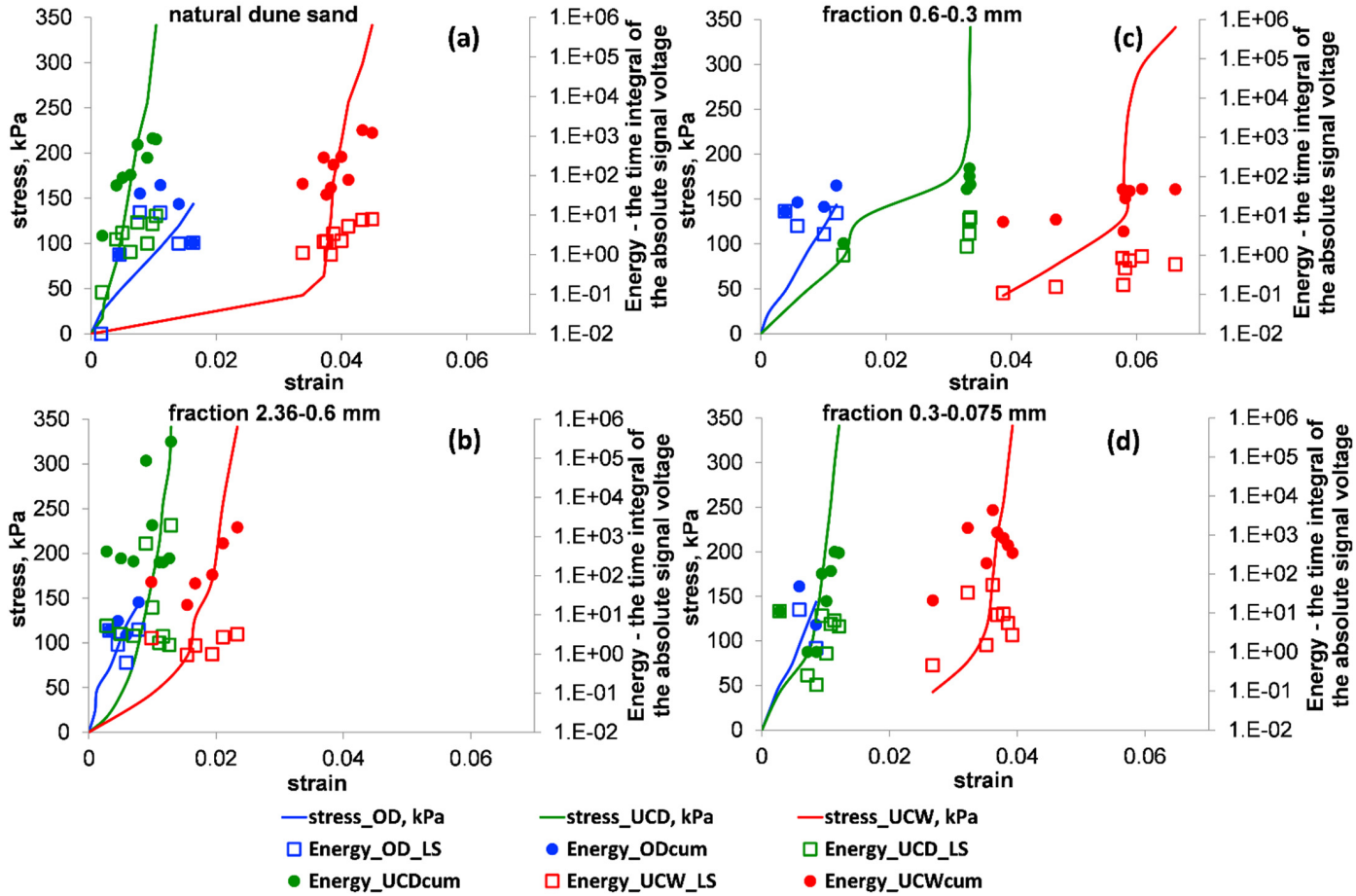

Figure 10. The stress–strain relationships (solid curves) vs. the energy values for the OD (blue), UCD (green) and UCW (red) tests. The empty squares and the full circles denote the values of the average (index = LS) and cumulative (index = cum) energy for a loading stage, respectively. Panels (**a**–**d**) illustrate the results for natural dune sand and its three extracted fractions: 2.36–0.6, 0.6–0.3, and 0.3–0.075 mm, respectively. Note that in the used number format, the notation "E±xx" is part of a scientific notation and corresponds to "$\cdot 10^{\pm xx}$".

3.3.5. Duration

The AE results in terms of the (signal) duration parameter are shown in Figure 11. The information extracted from Figure 11 is summarized as follows. The values of the average signal duration were quite unchangeable (~100 μs) with only one exception (UCD test, Figure 11b), with the coarsest fraction loading (in the range of 0.01–0.1 s) under relatively high stress (200–350 kPa). The highest value of the cumulative signal duration (for a load stage) was measured for the coarsest fraction during the UCD test as well (Figure 11b). During the OD and UCW tests, the parameter range was 10^2–10^5 μs, with the general tendency to increase with the rise in the stress level, while the minor values were measured during the OD tests (colored in blue). Note that the maximum value of the parameter was not generally synchronized with the maximum stress. Analysis of the results of the UCW test portrayed that the spread of signal duration values was lesser in the wet samples than in the dry ones.

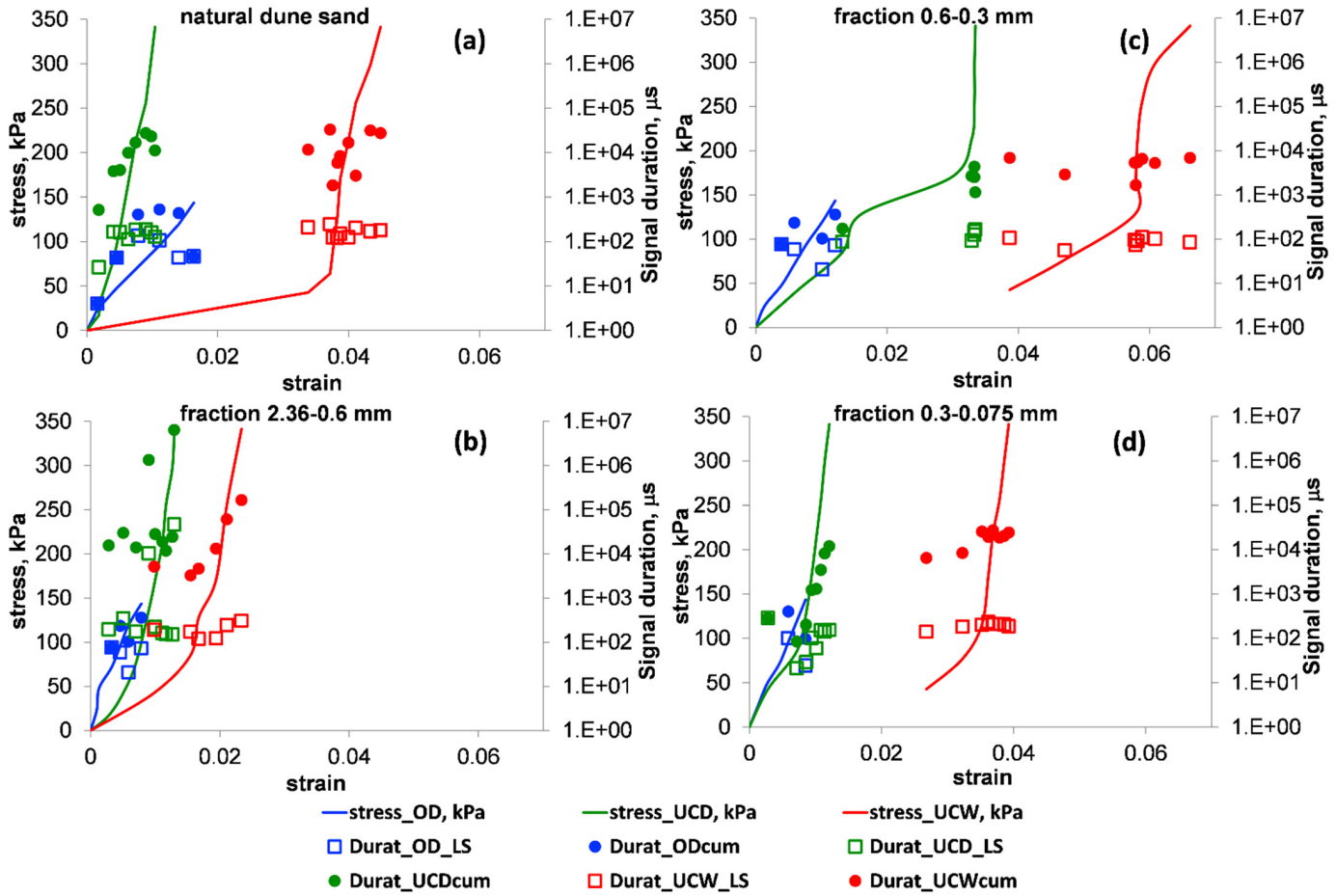

Figure 11. The stress–strain relationships (solid curves) vs. the values of the signal duration (Durat) for the OD (blue), UCD (green) and UCW (red) tests. The empty squares and the full circles denote the values of the average (index = LS) and cumulative (index = cum) signal durations for a loading stage, respectively. Panels (**a**–**d**) present the results for natural dune sand and its three extracted fractions: 2.36–0.6, 0.6–0.3 and 0.3–0.075 mm, respectively. Note that in the used number format, the notation "E±xx" is part of a scientific notation and corresponds to "$\cdot 10^{\pm xx}$".

3.3.6. Amplitude

The AE results in terms of the (signal) amplitude parameter are shown in Figure 12. One can observe from Figure 12 that the average amplitude values ranged from 10 to 100 dB for all studied samples during all tests. Additionally, an increase in the stress level was followed by an increase in the cumulative signal amplitude. This trend was very weak for the medium sand fraction (0.6–0.3 mm) during the UCW test (Figure 12c).

3.3.7. Average Frequency

The AE results in terms of the average frequency (Afreq) parameter are shown in Figure 13, from which one can conclude that the average frequency values did not depend on the stress–strain level for all studied samples and experiment types, probably due to signal filtering (see Section 2.1). Moreover, an increase in the stress level was followed by an increase in the cumulative value of the parameter, probably via an increase in the number of AE hits (see also Figure 7).

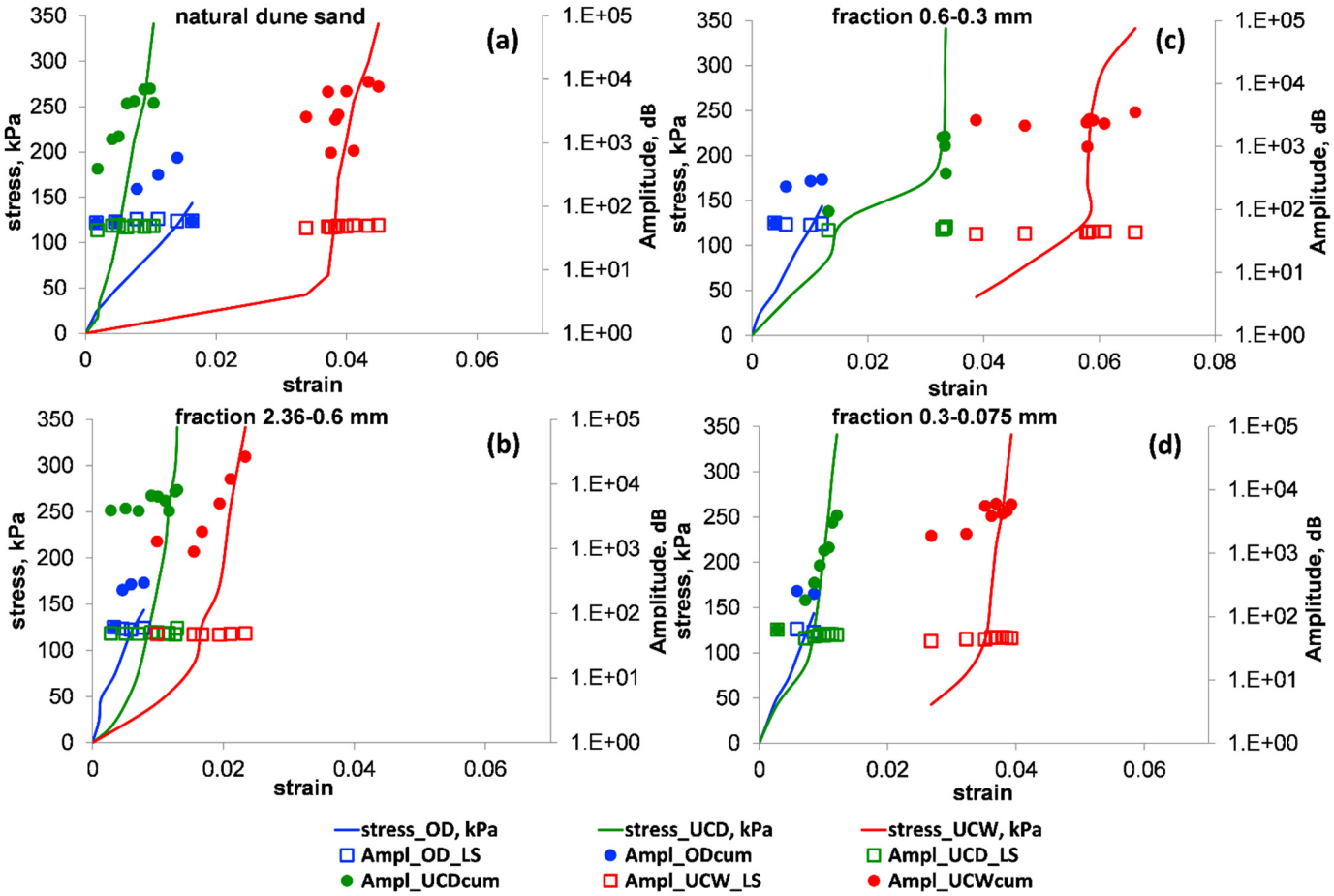

Figure 12. The stress–strain relationships (solid curves) vs. the values of the signal amplitude (Ampl) for the OD (blue), UCD (green) and UCW (red) tests. The empty squares and the full circles denote the values of the average (index = LS) and cumulative (index = cum) signal amplitudes for a loading stage, respectively. Panels (**a**–**d**) show the results for natural dune sand and its three extracted fractions: 2.36–0.6, 0.6–0.3 and 0.3–0.075 mm, respectively. Note that in the used number format, the notation "E±xx" is part of a scientific notation and corresponds to "$\cdot 10^{\pm xx}$".

3.3.8. Peak Number

The AE results in terms of the peak number (PCNTS) parameter are shown in Figure 14. Specifically, one can observe the following. The average peak number did not depend on the stress–strain level for all studied samples and experiment types. The exception was the deformation of the coarsest fraction, where two spikes of the parameter were noted under a relatively high stress of 300–350 kPa. An increase of the sum peak number for each loading stage mainly occurred for all studied samples, while the most intensive increase appeared for the coarsest dry sample (Figure 14b). This trend was very weak during the UCW tests with natural dune sand (Figure 14a) and two fine fractions (Figure 14c,d).

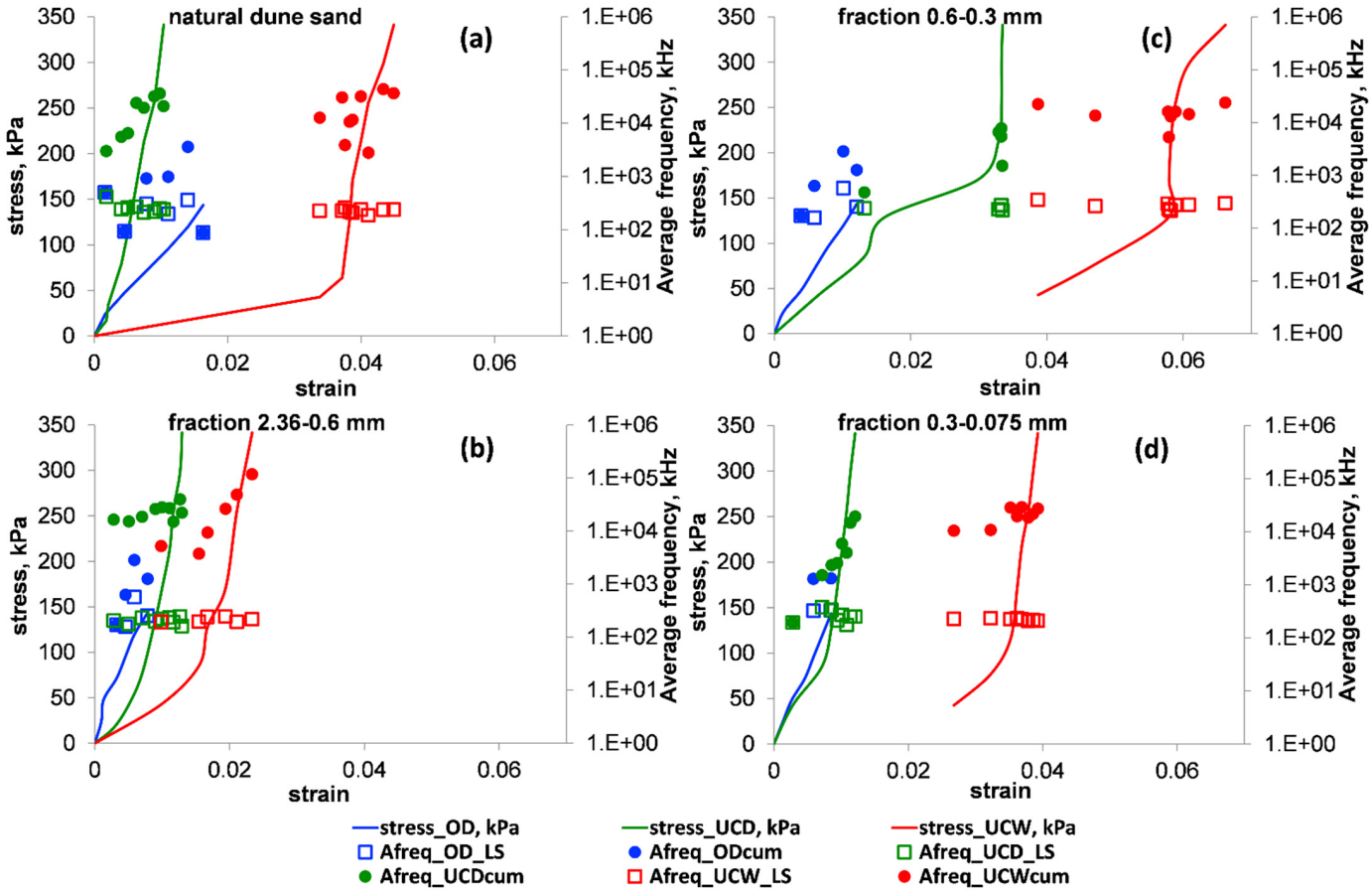

Figure 13. The stress–strain relationships (solid curves) vs. the values of the signal average frequency (Afreq) for the OD (blue), UCD (green) and UCW (red) tests. The empty squares and the full circles denote the values of the average (index = LS) and cumulative (index = cum) signal average frequencies for a load stage, respectively. Panels (**a**–**d**) illustrate the results for natural dune sand and its three extracted fractions: 2.36–0.6, 0.6–0.3 and 0.3–0.075 mm, respectively. Note that in the used number format, the notation "E±xx" is part of a scientific notation and corresponds to "$\cdot 10^{\pm xx}$".

3.3.9. Absolute Energy

The AE results in terms of the absolute energy (AbsEnergy) parameter are shown in Figure 15. One can draw the following conclusions from Figure 15. The average values of the absolute energy increased with a stress increase, mainly in subzone b. It was quite independent of the strain level (comparing the corresponding dry and wet experiments). The largest values were observed for the natural sand sample (dune) and the coarsest fraction (up to 10^7–10^8 aJ)—shown in Figure 15a,b—for the UCD test. Furthermore, the cumulative value of the parameter increased as well with the stress growth for all sand samples under study.

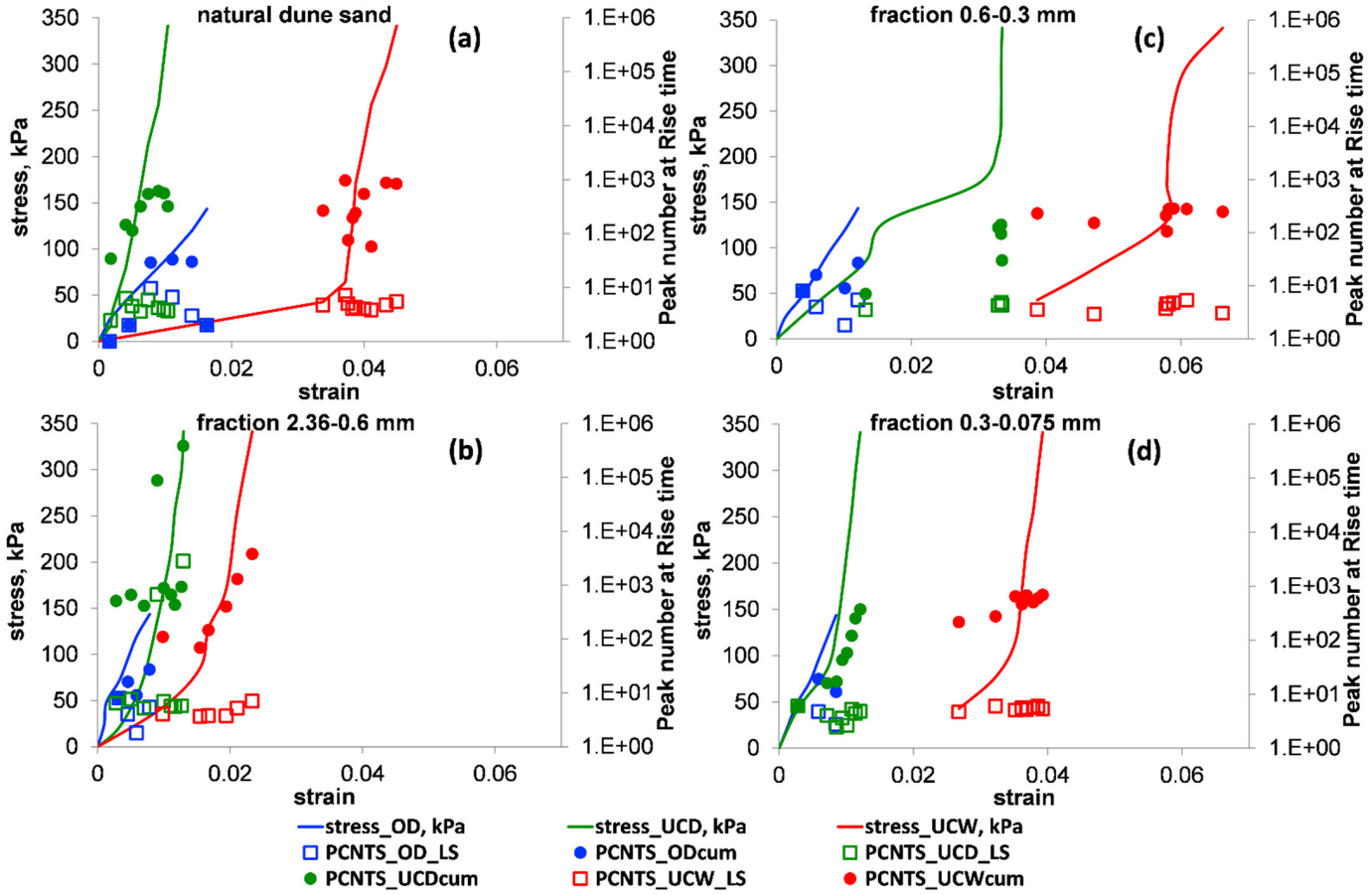

Figure 14. The stress–strain relationships (solid curves) vs. the values of the peak number (PCNTS) for the OD (blue), UCD (green) and UCW (red) tests. The empty squares and the full circles denote the values of the average (index = LS) and cumulative (index = cum) PCNTS for a load stage, respectively. Panels (**a**–**d**) present the results for natural dune sand and its three extracted fractions: 2.36–0.6, 0.6–0.3 and 0.3–0.075 mm, respectively. Note that in the used number format, the notation "E±xx" is part of a scientific notation and corresponds to "$\cdot 10^{\pm xx}$".

3.3.10. Summary of AE Results

Table 1 demonstrates the comparison of the sensitivity of different parameters to a stress increase. The symbols +, -, +/- and -/+ in Table 1 imply that a parameter is sensitive to a stress level increase, insensitive to a stress level increase, more sensitive than insensitive (it was found to be sensitive in the majority of the tests) and more insensitive than sensitive (it was found to be insensitive in the majority of the tests), respectively. Analysis of Table 1 indicated that the parameters which were the most sensitive to stress increases were the AE hit number and absolute energy (both average and cumulative), while the energy and rise time were also sensitive but only for the dry sand samples. Regarding the other six parameters, it was seen that their cumulative changes were probably due to their dependence on the number of AE hits.

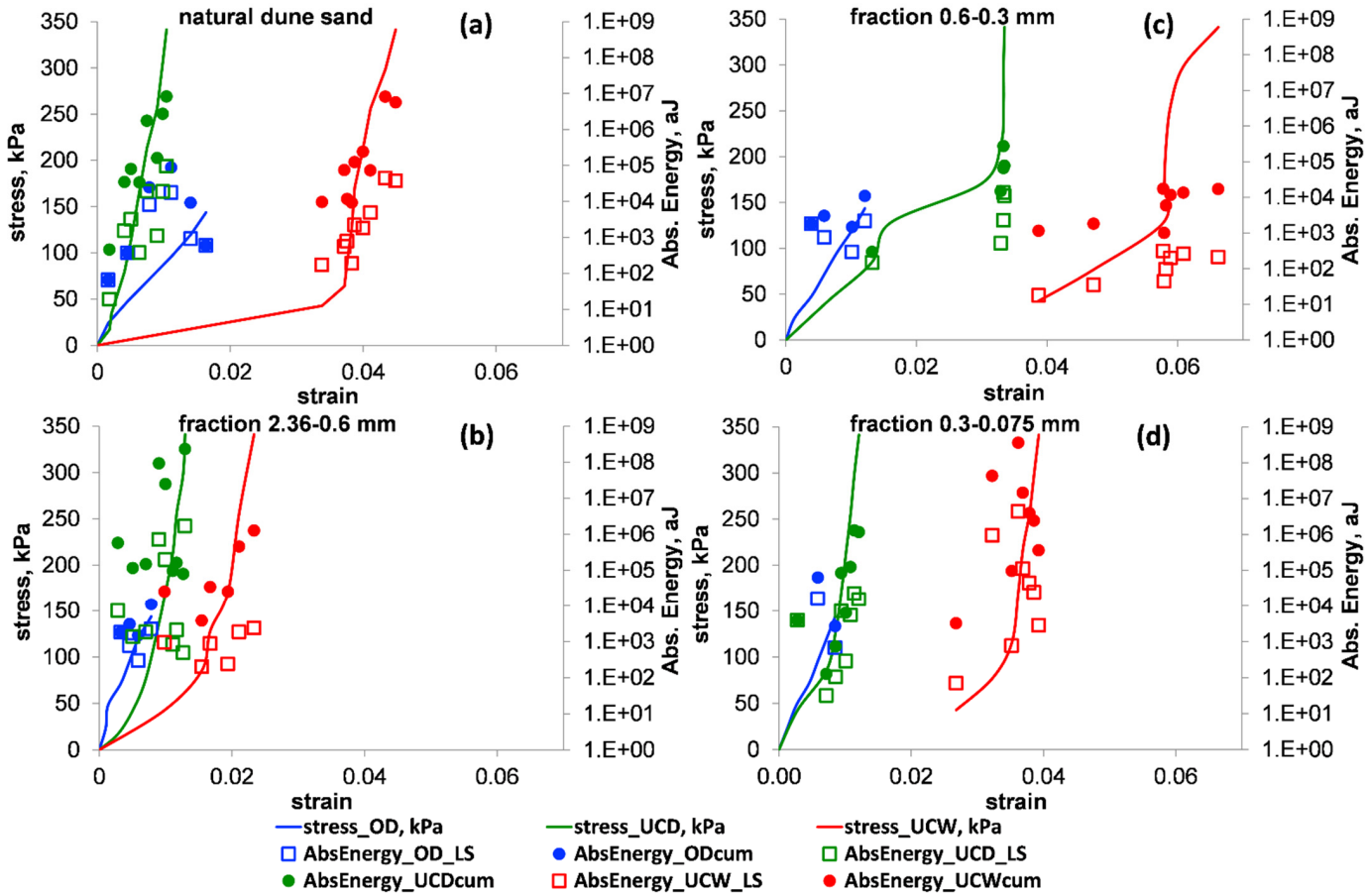

Figure 15. The stress–strain relationships (solid curves) vs. the values of the absolute energy (AbsEnergy) for the OD (blue), UCD (green) and UCW (red) tests. The empty squares and the full circles denote the values of the average (index = LS) and cumulative (index = cum) AbsEnergy for a loading stage, respectively. Panels (**a**–**d**) show the results for natural dune sand and its three extracted fractions: 2.36–0.6, 0.6–0.3 and 0.3–0.075 mm, respectively. Note that in the used number format, the notation "E±xx" is part of a scientific notation and corresponds to "$\cdot 10^{\pm xx}$".

Table 1. Summary of AE measurement results. For the interpretations of the +, -, +/- and -/+ symbols, refer to the main text.

Parameter	Average Value of the Parameter for a Loading Stage (Sensitivity to Stress Level)			Cumulative Value of the Parameter for a Loading Stage (Sensitivity to Stress Level)		
	OD	UCD	UCW	OD	UCD	UCW
AE hit number	+	+	+	+	+	+
Rise time	+	+	-/+	+	+	-/+
Counts	-	-/+	-/+	+	+	-/+
Energy	+	+	+/-	+	+	+/-
Duration	-	-	-	+	+	+/-
Amplitude	-	-	-	+	+	+/-
Average frequency	+	-	-	+	+	-/+
Peak number	-	-/+	-	+	+	+/-
Absolute energy	+	+	+/-	+	+	+/-

4. Conclusions

This study highlights differences in the stress–strain behavior of four types of sand under low stress loading via the comparison of their stress–strain diagrams in two types of loading tools (an oedometer and a uniaxial compression machine), as well as their US and AE characteristics. A wide range of sand grain sizes (0.075–4.75 mm) was utilized for the study. Analysis of the sensitivities of different time domain AE parameters to the stress–strain changes was performed.

By comparing the OD and UCD results for the US measurements, we conclude that the value of the HtD affected the results of the compression tests, primarily due to changes in the soil stiffness. The lower the HtD was, the stiffer the soil sample was due to the confining stress (triaxial stress mode), which implied restriction in the mobility of soil particles. The value of the confining stress can be estimated via the ratio of the lateral stress to the vertical stress, being $K_0 = 1 - \sin\phi$ (lateral stress factor at rest), where ϕ is the friction angle. For quartz sand, ϕ is generally in the range of 20–30° ($\phi = -12.963 \cdot d + 29.778$, where ϕ is expressed in degrees and d is the particle size in mm, and the regression has been extracted from Figures 6–9. in [17]). The increase in the confining stress σ_3 can be of the order of $\sigma_3 = \sigma_1 \cdot K_0$, where $K_0 = 0.5,\ 0.66$. The confining stress value under compression must be taken into account for the short samples (HtD < 2), while it is known to disappear in the middle part of the long cylindrical samples (HtD $\geq$ 2). As we noted above, HtD < 1 in the OD experiments while it was ≈2 in the UCD and UCW tests, implying that the sand samples were much stiffer in the OD experiments (being under quasi-triaxial stress conditions) than in the UCD and UCW tests. The stiffer the soil was, the higher the value of the P wave speed was. This is the reason why similar P wave velocities were achieved at a much lower applied stress during the OD experiments in comparison with the UCD and UCW tests.

By comparing the UCD and UCW results for the US measurements, we conclude that during both experiments, the range of the P wave speed was similar for all types of samples tested, while the value of the induced strain was much higher during experiments with wet sand samples relative to those using dry ones. The latest results can be explained by a decrease in friction between the soil particles with a subsequent increase in its compressibility (mainly due to the presence of a wide subzone a). Concerning the similarity of P wave speed values during the UCD and UCW experiments, it is known [36] that the value of the P wave speed of a wet medium can be estimated as follows:

$$\frac{1}{\overline{V}_p} = \frac{n}{V_w} + \frac{1-n}{V_p^{dry}} \tag{2}$$

where $\overline{V}_p$, V_p^{dry} and $V_w = 1481\ m/s$ are values of the P wave speed in wet and dry soils and water, respectively, and n is the soil porosity value. Substitution of the values of porosity of our samples, of the P wave speed obtained by our experiments and of the P wave speed known for water into Equation (2) yields a difference between the values of the P wave speed in dry and wet sand samples of about 4%, which is generally consistent with the results of our observations.

Regarding the AE measurement results, we conclude that the similarity of the changes in the AE hit number with a stress increase is consistent with the results noted by [15,20,21,30]: the higher the stress level is, causing more friction between the sand particles, the more AE events there are during their movement. Comparison of the results of the OD and UCD tests was also consistent with the results observed by [17,20,21,31], who noted that, at a similar stress level, stiffer specimens emit fewer acoustic signals due to the difference in compression modes. More AE signals in subzone a, registered in the wet sand experiments, were probably due to the higher mobility of the sand particles lubricated with water, inducing a higher number of AE events. However, it must be noted that the number of AE hits was still much lower in subzone a than in subzone b, which is also consistent with the observations of [17,20,21,31].

The following parameters of AE were shown to be the most sensitive to the stress increases: the AE hit number and the signal energy. Note the consistency of the last result with those from Mao et al. [16].

Author Contributions: Conceptualization, V.F. and S.M.P.; data curation, S.S.; formal analysis, V.F., S.M.P. and S.S.; methodology, V.F.; writing—original draft, V.F. and S.M.P.; writing—review and editing, V.F., S.M.P. and S.S. All authors have read and agreed to the published version of the manuscript.

Funding: This research was funded by the Ministry of Construction and Housing of Israel, Grant 3/2019, 4501851885.

Institutional Review Board Statement: The study did not require ethical approval.

Informed Consent Statement: Not applicable.

Data Availability Statement: All data generated and analyzed during this study are included in the article.

Acknowledgments: V.F. and S.S. would like to thank the Ministry of Construction and Housing of Israel for the financial support of the research (Grant 3/2019, 4501851885).

Conflicts of Interest: The authors declare no conflict of interest.

References

1. Hallbauer, D.K.; Wagner, H.; Cook, N.G.W. Some observations concerning the microscopic and mechanical behaviour of quartzite specimens in stiff, triaxial compression tests. *Int. J. Rock Mech. Min. Sci. Geomech. Abstr.* **1973**, *10*, 713–726. [CrossRef]
2. Kuksenko, V.S.; Manzikov, V.; Mansurov, V.A. Regularities in the development of microfocal rupture. *Izvesiya Earth Phys.* **1985**, *21*, 553–556.
3. Lockner, D.; Reches, Z. Nucleation and growth of faults in brittle rocks. *J. Geophys. Res. Solid Earth* **1994**, *99*, 18159–18173.
4. Guha, S.K. *Induced Earthquakes*; Kluwer Academic Publisher: Dordrecht, The Netherlands, 2000; p. 313.
5. Thompson, B.D.; Young, R.P.; Lockner, D.A. Fracture in westerly granite under AE feedback and constant strain rate loading: Nucleation, quasi-static propagation, and the transition to unstable fracture propagation. *Pure Appl. Geophys.* **2006**, *163*, 995–1019. [CrossRef]
6. Goebel, T.H.W.; Schorlemmer, D.; Becker, T.W.; Dresen, G.; Sammis, C.G. Acoustic emissions document stress changes over many seismic cycles in stick-slip experiments. *Geophys. Res. Lett.* **2013**, *40*, 2049–2054. [CrossRef]
7. Goodfellow, S.D.; Young, R.P. A laboratory acoustic emission experiment under in situ conditions. *Geophys. Res. Lett.* **2014**, *41*, 3422–3430. [CrossRef]
8. McLaskey, G.C.; Lockner, D.A. Calibrated acoustic emission system records M 23.5 to M 28 events generated on a saw-cut granite sample. *Rock Mech. Rock Eng.* **2016**, *49*, 4527–4536. [CrossRef]
9. Frid, V.; Shabarov, A. Modern principles of nondestructive stress monitoring in mine workings-Overview. In *EUROCK2018: Geomechanics and Geodynamics of Rock Masses, Proceedings of the 2018 European Rock Mechanics Symposium, Saint Petersburg, Russia, 22–26 May 2018*; Taylor & Francis Group: London, UK, 2018; pp. 513–518.
10. Rehes, Z. Mechanisms of slip nucleation during earthquakes. *Earth Planet. Sci. Lett.* **1999**, *170*, 475–486. [CrossRef]
11. Liang, Y.; Li, Q.; Gu, Y.; Zou, Q. Mechanical and acoustic emission characteristics of rock: Effect of loading and unloading confining pressure at the postpeak stage. *J. Nat. Gas Sci. Eng.* **2017**, *44*, 54–64. [CrossRef]
12. Grosse, C.U.; Ohtsu, M. (Eds.) *Acoustic Emission Testing*; Springer: Berlin/Heidelberg, Germany, 2008.
13. Ulusay, R. (Ed.) *The ISRM Suggested Methods for Rock Characterization, Testing and Monitoring: 2007–2014*; Springer: Cham, Switzerland, 2015. [CrossRef]
14. ASTM E1932-12(2017). *Standard Guide for Acoustic Emission Examination of Small Parts*; ASTM International: West Conshohocken, PA, USA, 2017.
15. Michlmayr, G.; Cohen, D.; Or, D. Sources and characteristics of acoustic emissions from mechanically stressed geologic granular media—A review. *Earth-Sci. Rev.* **2012**, *112*, 97–114. [CrossRef]
16. Mao, W.; Yang, Y.; Lin, W. An acoustic emission characterization of the failure process of shallow foundation resting on sandy soils. *Ultrasonics* **2019**, *93*, 107–111. [CrossRef]
17. Lambe, T.W.; Whitman, R.V. *Soil Mechanics*; John Wiley and Sons Inc.: New York, NY, USA, 1969.
18. Fernandes, F.; Syahrial, A.I.; Valdes, J.R. Monitoring the oedometric compression of sands with acoustic emissions. *Geotech. Test. J.* **2020**, *33*, 410–415. [CrossRef]
19. Lin, W.; Liu, A.; Mao, W. Use of acoustic emission to evaluate the micro-mechanical behavior of sands in single particle compression tests. *Ultrasonics* **2019**, *99*, 105962. [CrossRef]
20. Lin, W.; Liu, A.; Mao, W.; Koseki, J. Acoustic emission characteristics of a dry sandy soil subjected to drained triaxial compression. *Acta Geotech.* **2020**, *15*, 2493–2506. [CrossRef]

21. Naderi-Boldaji, M.; Bahrami, M.; Keller, T.; Or, D. Characteristics of acoustic emissions from soil subjected to confined uniaxial compression. *Vadose Zone J.* **2017**, *16*, 1–12. [CrossRef]
22. Munoz-Ibanez, A.; Delgado-Martın, J.; Grande-Garcıa, E. Acoustic emission processes occurring during high-pressure sand compaction. *Geophys. Prospect.* **2019**, *67*, 761–783. [CrossRef]
23. De Cola, F.; Quino, G.; Dragnevski, K.; Petrinic, N. An extended in-situ method to improve the understanding of fracture mechanics of granular materials using sound measurements. *Eur. J. Mech. A Solids* **2019**, *76*, 1–12. [CrossRef]
24. ASTM D2845-08(2008). *Standard Test Method for Laboratory Determination of Pulse Velocities and Ultrasonic Elastic Constants of Rock*; ASTM International: West Conshohocken, PA, USA, 2008.
25. Stephenson, R.W. Ultrasonic testing for determining dynamic soil mocduli. In *Dynamic Geotechnical Testing*; Silver, M., Tiedemann, D., Eds.; ASTM International: West Conshohocken, PA, USA, 1978; pp. 179–195. [CrossRef]
26. Zimmer, M.A.; Prasad, M.; Mavko, G.; Nur, A. Seismic velocities of unconsolidated sands: Part 1—Pressure trends from 0.1 to 20 MPa. *Geophysics* **2007**, *72*, E1–E13. [CrossRef]
27. Chen, Y.; Irfan, M.; Uchimura, T. Estimation of elastic wave velocity through unsaturated soil slope as function of water content and shear deformation. *Soils Found.* **2019**, *59*, 2180–2194. [CrossRef]
28. Frid, V.; Potirakis, S.M.; Shulov, S. Effect of soil loading and unloading on its acoustic behavior. *Proceedings* **2020**, *67*, 20. [CrossRef]
29. Luo, S.S.; Ibraim, E.; Diambra, A. Acoustic emission monitoring of crushing of an analogue granular material. *Géotechn. Lett.* **2019**, *9*, 1–9. [CrossRef]
30. Smith, A.; Dixon, N. Acoustic emission behaviour of dense sands. *Géotechnique* **2019**, *69*, 1107–1122. [CrossRef]
31. Smith, A.H.; Heather-Smith, J.; Dixon, N.; Flint, J.A.; Pennie, D. Acoustic emission generated by granular soil-steel structure interaction. *Géotechn. Lett.* **2020**, *10*, 1–9. [CrossRef]
32. Xiao, Y.; Wang, L.; Jiang, X.; Matthew Evans, T.; Stuedlein, A.W.; Liu, H. Acoustic emission and force drop in grain crushing of carbonate sands. *Geotech. Geoenviron. Eng.* **2019**, *145*, 04019057. [CrossRef]
33. Hangx, S.J.T.; Brantut, N. Micromechanics of high-pressure compaction in granular quartz aggregates. *J. Geophys. Res. Solid Earth* **2019**, *124*, 6560–6580. [CrossRef]
34. Sharma, A.; Penumadu, D. Role of particle shape in determining tensile strength and energy release in diametrical compression of natural silica grains. *Soils Found.* **2020**, *60*, 1299–1311. [CrossRef]
35. ASTM D4959-00. *Standard Test Method for Determination of Water (Moisture) Content of Soil by Direct Heating*; ASTM International: West Conshohocken, PA, USA, 2016.
36. Rgevsky, V.V.; Novik, G.Y. *Foundations of Rock Physics*; Nedra: Moscow, Russia, 1978.